equations is shown in Figure 4. The transconductance values are evaluated at a V_{DS} of 28 V. The transconductance is well modeled for the values before the V_{pk} and a good approximation was obtained V_{GS} biasing beyond V_{pk}. Transconductance beyond V_{pk} was well predicted with an error of less than 10% with the exception of the transconductance at V_{GS} of 0 V having an error of 13%.

4. CONCLUSION

A current model derived from the modified Chalmer's equations to characterize the active current of an active device was proposed. The proposed model improves the modeling capability of the current equations for GaN based HEMT devices and the straightforward parameters extraction procedures add to the merits of the proposed equations. The equation improves the modeling of the output conductance across all the V_{GS} biasing points and provides a more practical and physical representation of the device performance at high V_{DS} voltages. Divergence of transconductance was highlighted illustrating the effects if there is no additional function control the output conductance value at high applied V_{DS} biasing. Comparison between the simulated and experimental data for the active current and evaluated gm verified the validity of the proposed equations.

REFERENCES

1. L. Dunleavy, et al., Modeling GaN: Powerful but challenging, IEEE Microwave Mag 11 (2010), 82–96.
2. I. Angelov, et al., A new empirical nonlinear model for HEMT and MESFET devices, IEEE Trans Microwave Theory Tech 40 (1992), 2258–2266.
3. W.R. Curtice, et al., A nonlinear GaAs FET model for use in the design of output circuits for power amplifiers, IEEE Trans Microwave Theory Tech 33 (1985), 1383–1393.
4. Agilent Technologies, ICCAP software documentation, Palo Alto, CA: Agilent Technologies Inc., 2009.
5. I. Angelov, et al., On the large-signal modeling of AlGaN/GaN HEMTs and SiC MESFETs, In: Proceedings of the 13th GASS Symposium, Paris, 2005, pp. 309–312.
6. I. Angelov, et al., Large-signal modeling and comparison of AlGaN/GaN HEMTs and SiC MESFETs, In: Asia-Pacific Microwave Conference (APMC), Yokohama, Japan, December 2006, pp. 279–282.
7. J. Deng, et al., Temperature-dependent rf large-signal model of GaN-based MOSHFETs, IEEE Trans Microwave Theory Tech, 56 (2008), 2709–2716.
8. I. Angelov, et al., Extensions of the Chalmers nonlinear HEMT and MESFET model, IEEE Trans Microwave Theory Tech 44 (1996), 1664–1674.
9. H. Zhou, et al., An improved large-signal I-V model of GaN model, In: International Conference on Computational Problem-Solving (ICCP), 2012, pp. 284–286.
10. Y. Liu, et al., AlGaN/GaN HEMT large signal nonlinear compact model accounting for thermal effects and trapping dispersion, In: IEEE Compound Semiconductor Integrated Circuit Symposium (CSICS), 2013, pp. 1–5.
11. D. Liu, et al., GaN HEMT large-signal model research, In: International Workshop on Microwave and Millimeter Wave Circuits and System Technology (MMWCST), 2012, pp. 1–5.
12. L.S. Liu, et al., Electrothermal large-signal model of III-V FETs accounting for frequency dispersion and charge conservation, In: IEEE MTT-S International Microwave Symposium Digest, 2009, pp. 749–752.
13. L.S. Liu, et al., Electrothermal large-signal model of III-V FETs including frequency dispersion and charge conservation, IEEE Trans Microwave Theory Tech 57 (2009), 3106–3117.
14. A.E. Parker, et al., Measurement and characterization of HEMT dynamics, IEEE Trans Microwave Theory Tech 49 (2001), 2105–2111.
15. A. N. Ernst, et al., Dynamics of the kink effect in In-AlAs/InGaAs HEMTs, IEEE Electron Device Lett 18 (1995), 613–615.
16. R.T. Webster, et al., Impact ionization in In-AlAs/InGaAs/InAlAs HEMTs, IEEE Trans Microwave Theory Tech 45 (1997), 1563–1571.
17. B.M. Green, et al., Validation of an analytical large signal model for AlGaN/GaN HEMT's on SiC substrates, In: IEEE Conference on High Performance Devices, 2000, pp. 237–241.
18. B.M. Green, et al., Validation of an analytical large signal model for AlGaN/GaN HEMTs, In: IEEE MTT-S International Microwave Symposium Digest, Vol. 2, Boston, MA, 2000, pp. 761–764.
19. M. Berroth, et al., Advanced large-signal modeling of GaN HEMTs, In: IEEE Lester Eastman Conference on High Performance Devices, 2002, pp. 172–180.

AN ULTRATHIN QUAD-BAND POLARIZATION-INSENSITIVE WIDE-ANGLE METAMATERIAL ABSORBER

Devkinandan Chaurasiya, Saptarshi Ghosh, Somak Bhattacharyya, and Kumar Vaibhav Srivastava
Department of Electrical Engineering, Indian Institute of Technology Kanpur, Kanpur, Uttar Pradesh, India; Corresponding author: joysaptarshi@gmail.com

Received 21 July 2014

ABSTRACT: *In this article, an ultrathin quad-band polarization-insensitive wide-angle metamaterial absorber has been presented. The proposed structure consists of a periodic array of concentric square and circular rings imprinted on grounded FR-4 dielectric substrate. The simulated result shows that the structure has four discrete absorption peaks at 3.91, 5.16, 7.10, and 9.16 GHz with peak absorptivities of 99.35, 98.04, 99.85, and 99.78%, respectively. The proposed structure is symmetric in design providing nearly unity absorption for all polarization angles under normal incidence. It also shows high absorption (∼90%) for wide incident angles upto 45° for both transverse electric and transverse magnetic polarizations. By illustrating surface current distribution, the absorption mechanism of different parts of the proposed structure has been analyzed. Finally, the structure has been fabricated and the measured results are in good agreement with the simulated responses. The designed quad-band absorber is easy to manufacture and can be used in various potential applications.* © 2015 Wiley Periodicals, Inc. Microwave Opt Technol Lett 57:697–702, 2015; View this article online at wileyonlinelibrary.com. DOI 10.1002/mop.28928

Key words: *metamaterial; microwave absorber; polarization-insensitive; quad-band*

1. INTRODUCTION

In recent years, electromagnetic (EM) metamaterials (MTMs) [1] have drawn significant research interests due to their peculiar properties. Several potential applications, such as perfect lens [2], cloaking [3], antenna miniaturization [4], and so forth have been proposed over the EM spectrum covering from microwave to visible regimes. One of the major applications is to design perfect MTM absorbers [5], which can produce near-unity absorption by tuning the effective electric permittivity and magnetic permeability of the homogenized structure. In addition, they also exhibit versatile distinct features over conventional material based absorbers such as ultrathin nature, flexible manipulation of constitutive EM properties, wide incident angle absorption, polarization insensitivity, and so on. Till date, various designs on MTM absorbers have been investigated

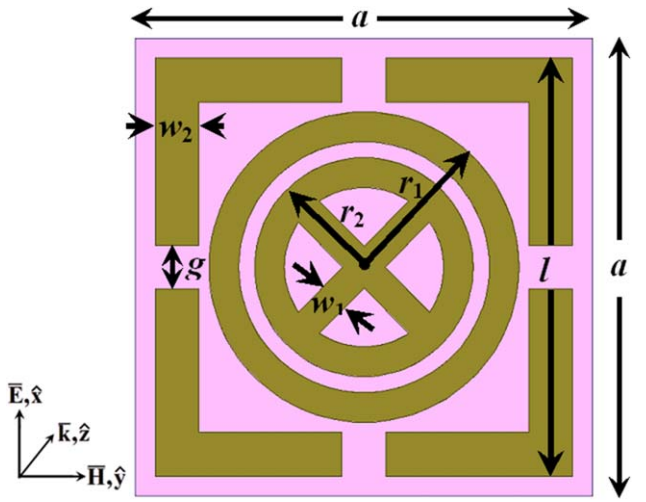

Figure 1 Front view of the unit cell of the proposed structure with geometrical dimensions: $a = 23$, $l = 21$, $w_1 = 1.5$, $w_2 = 2.2$, $r_1 = 7.8$, $r_2 = 5.5$, and $g = 2.2$ (unit: mm). [Color figure can be viewed in the online issue, which is available at wileyonlinelibrary.com]

exhibiting different characteristics, such as single-band [6–8], dual-band [9,10], triple-band [11,12], bandwidth enhanced [13–15], and even broadband operations [16,17], with most of them being polarization-insensitive and wide-angle absorptive. However, there is still a lack of sufficient progress toward the design and implementation of quad-band MTM absorber, which can be used in spectroscopic detection and phase imaging of hazardous materials and prohibited drugs [18]. Although some articles have proposed quad-band absorption by incorporating a set of resonant geometries with scaled dimensions, but they suffer from the constraint of large unit-cell size [19].

In this article, an ultrathin quad-band MTM absorber has been proposed with simultaneous polarization insensitivity and wide-angle absorption characteristics. The proposed structure comprises of a square outer ring with four splits, and two inner circular rings with the smaller one being cross connected. The simulated result shows four distinct absorption peaks at 3.91, 5.16, 7.10, and 9.16 GHz with peak absorptivities of 99.35, 98.04, 99.85, and 99.78%, respectively. The impedance characteristics and surface current distributions have been presented to analyze the absorption mechanism of the structure. Moreover, the proposed structure shows high absorption for all polarization angles under normal incidence as well as for wide incident angles upto 45° for both transverse electric (TE) and transverse magnetic (TM) polarizations. The experimental measurements are in good agreement with the simulated responses indicating that the proposed structure can be used as an ultrathin, polarization-insensitive, wide-angle, and quad-band MTM absorber in various absorber applications.

2. DESIGN AND SIMULATED RESULTS

Figure 1 shows the unit-cell geometry of the proposed structure, which consists of a top metallic layer and bottom ground plane with a dielectric substrate between them. The top layer comprises of an outer square ring with four splits, and two inner circular rings with the smaller one being cross connected. Commercially available FR-4 substrate (relative permittivity $\varepsilon_r = 4.2$ and dielectric loss tangent tan $\delta = 0.02$) with thickness of 1 mm has been considered as dielectric. Both the top and bottom layers are made of copper ($\sigma = 5.8 \times 10^7$ S/m) having thickness of 0.035 mm.

When a plane wave is incident on the structure, the absorptivity $A(\omega)$ can be calculated as in (1), where $S_{11}(\omega)$, $S_{21}(\omega)$, and $A(\omega)$ are the reflection coefficient, transmission coefficient, and absorptivity, respectively, at an angular frequency ω. Since the bottom layer is completely copper laminated, the transmission coefficient S_{21} (ω) is zero, and hence (1) can be represented as

$$A(\omega) = 1 - |S_{11}|^2 - |S_{21}|^2 = 1 - |S_{11}|^2. \quad (1)$$

Therefore, when the input impedance $Z(\omega)$ of the structure is perfectly matched with free space impedance η_0, then the reflectivity gets minimized and absorptivity will be maximum as obtained from (2) [20]

$$S_{11} = \frac{Z(\omega) - \eta_0}{Z(\omega) + \eta_0}. \quad (2)$$

The structure is simulated with Ansys HFSS using periodic boundary conditions, showing four discrete absorption peaks at 3.91 GHz (S-band), 5.16 GHz (C-band), 7.10 GHz (C-band), and 9.16 GHz (X-band) with absorptivity of 99.35, 98.04, 99.85,

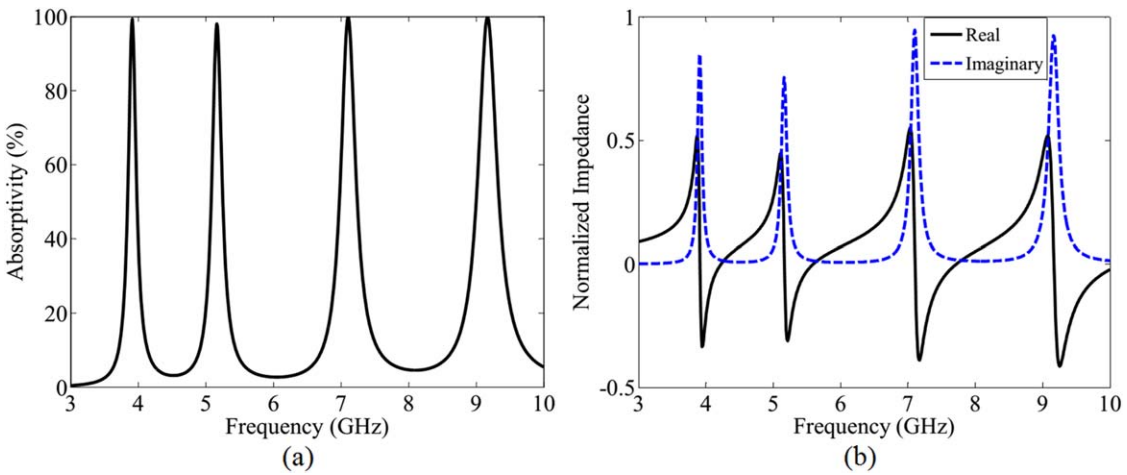

Figure 2 (a) Simulated absorptivity and (b) retrieved normalized input impedance of the proposed structure. [Color figure can be viewed in the online issue, which is available at wileyonlinelibrary.com]

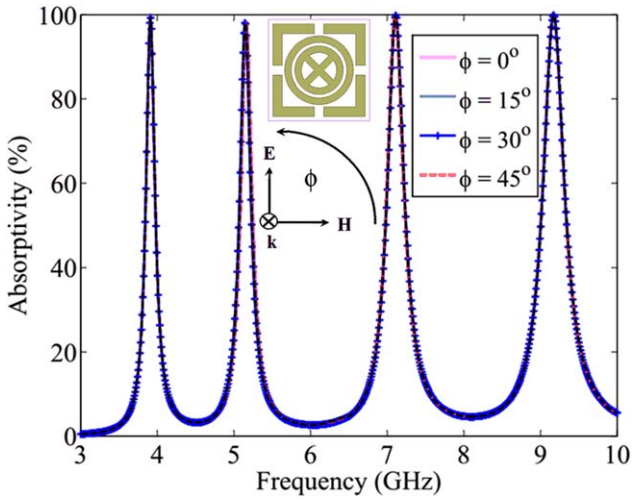

Figure 3 Simulated absorptivity for different polarization angles under normal incidence of the proposed structure. [Color figure can be viewed in the online issue, which is available at wileyonlinelibrary.com]

and 99.78%, respectively, as shown in Figure 2(a). As expected from (2), the normalized input impedance $Z(\omega)$ of the proposed structure matches closely with the free space impedance η_0 as shown in Figure 2(b). It is observed that the real parts of $Z(\omega)$ are close to unity, while the imaginary parts of $Z(\omega)$ are nearly zero for all the four absorption peaks, thus supporting the absorption phenomenon.

The structure is theoretically investigated under different angles of polarization as shown in Figure 3. Due to structural symmetry, the structure is studied only upto 45° angle of polarization, where it shows near-unity absorption for all the polarization angles under normal incidence.

Further, the structure has been examined under oblique angles of incidence for both TE and TM polarizations. In case of TE polarization, the electric field direction is kept constant, whereas the magnetic field and wave vector directions have been rotated from 0° to 45°. On the contrary, the magnetic field direction is remained fixed, while the other two vectors are varied in case of TM polarization. In both the cases, the simulated absorptivity remains above 90% for all the four absorptivity frequencies as shown in Figures 4(a) and 4(b), respectively.

To analyze the absorption mechanism of the designed structure, the surface current distributions of the top and bottom surface have been shown at the four absorption frequencies in Figures 5 and 6, respectively. It is observed that at 3.91 GHz, surface current is mainly localized in the intermediate circular ring, whereas most of the currents are distributed in the inner most cross-connected ring at 7.10 GHz. The cross part provides an extra parallel path for the flow of surface current, and therefore, the effective inductance is decreased and consequently the absorption frequency is increased. The outer square ring with four splits at four sides are responsible for near-unity absorption

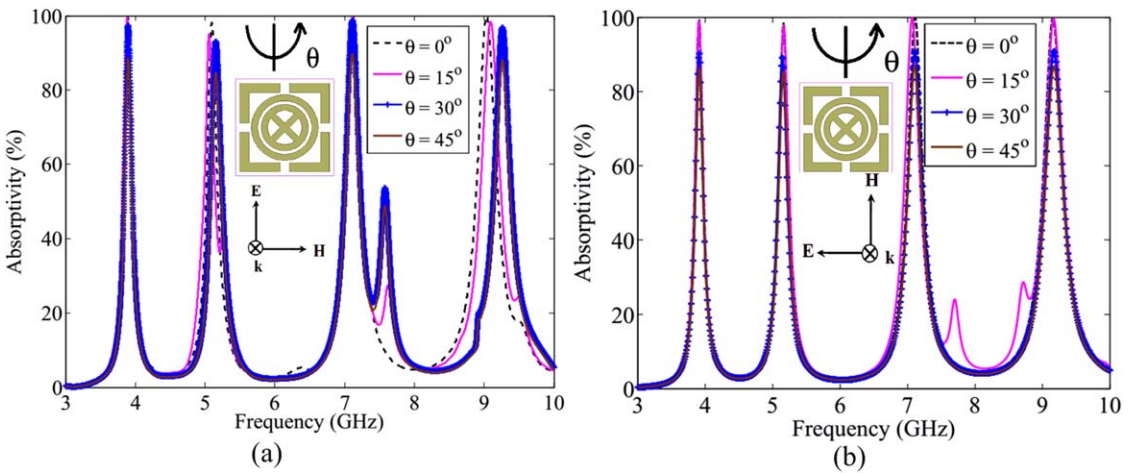

Figure 4 Simulated absorptivity under oblique incidence condition for (a) TE and (b) TM polarizations. [Color figure can be viewed in the online issue, which is available at wileyonlinelibrary.com]

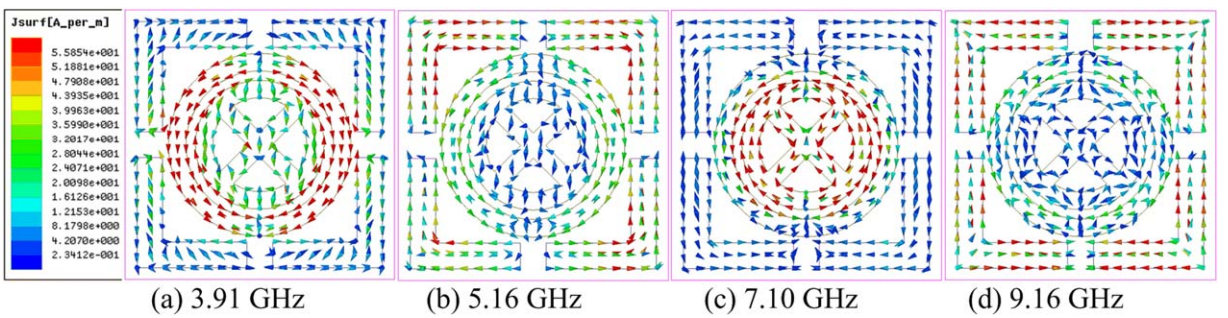

Figure 5 Surface current distributions at top surface at the frequencies of absorption. [Color figure can be viewed in the online issue, which is available at wileyonlinelibrary.com]

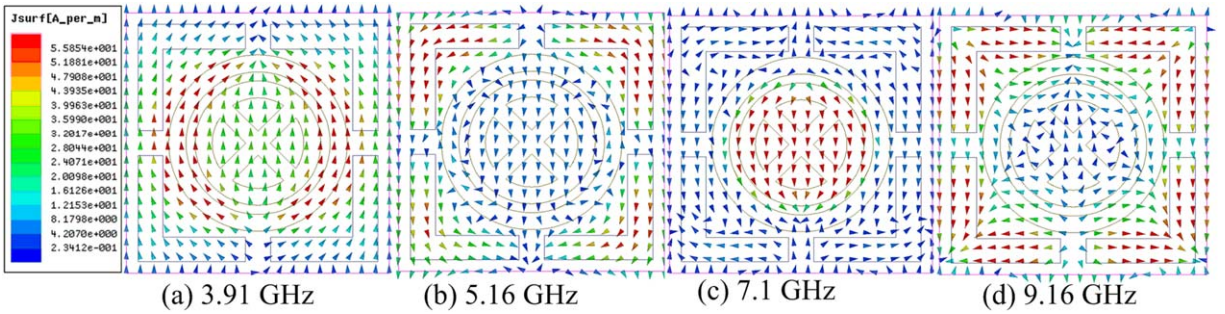

Figure 6 Surface current distributions at bottom surface at the frequencies of absorption. [Color figure can be viewed in the online issue, which is available at wileyonlinelibrary.com]

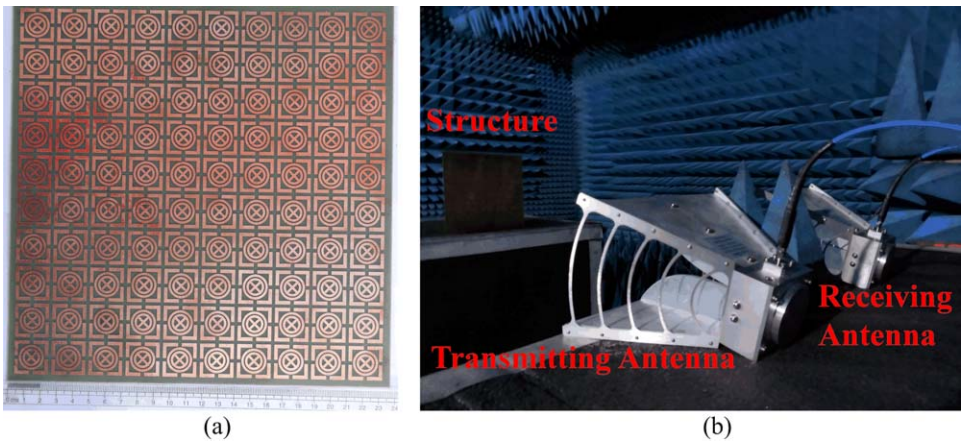

Figure 7 (a) Fabricated quad-band structure and (b) experimental arrangement within the anechoic chamber. [Color figure can be viewed in the online issue, which is available at wileyonlinelibrary.com]

at two different frequencies, viz. 5.16 and 9.16 GHz, unlike a single square ring (without splits) providing a single absorption frequency [21]. At 5.16 GHz, surface current is flowing from lower half to upper half in the outer square ring, whereas current is flowing from and toward the corners of the ring at 9.16 GHz. The three concentric rings thus exhibits four different absorption peeks. It is noteworthy that at all the four absorption frequencies, the top and bottom surface currents are in antiparallel direction, which constitute circulating loop around the incident magnetic field and forms magnetic excitation. Conversely, the top surface metallic patch array is electrically excited by the incident electric field. Both the excitations become significant at the absorption frequencies and near-unity absorption has been realized.

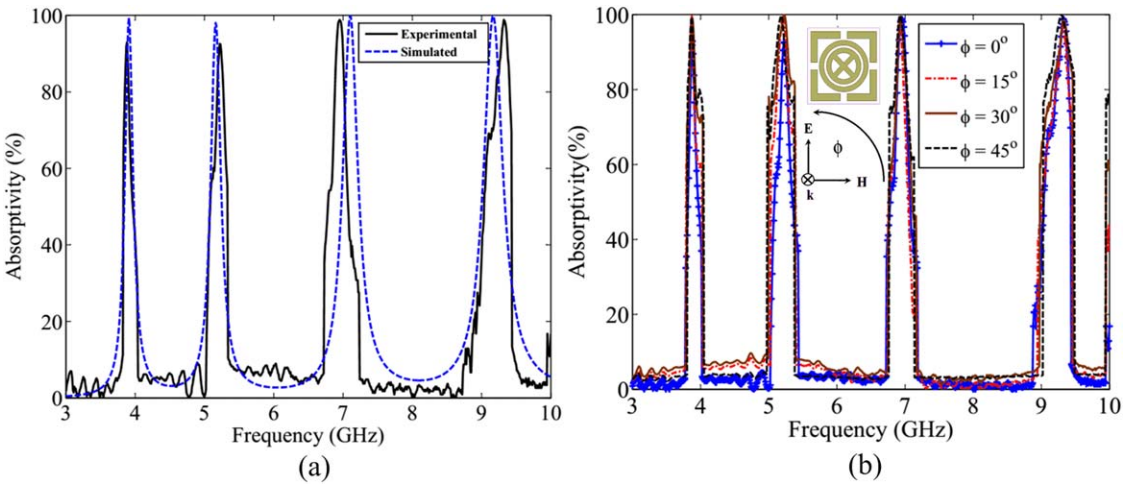

Figure 8 (a) Comparison of simulated and measured absorptivity plot for quad-band structure and (b) measured results for different polarization angles under normal incidence. [Color figure can be viewed in the online issue, which is available at wileyonlinelibrary.com]

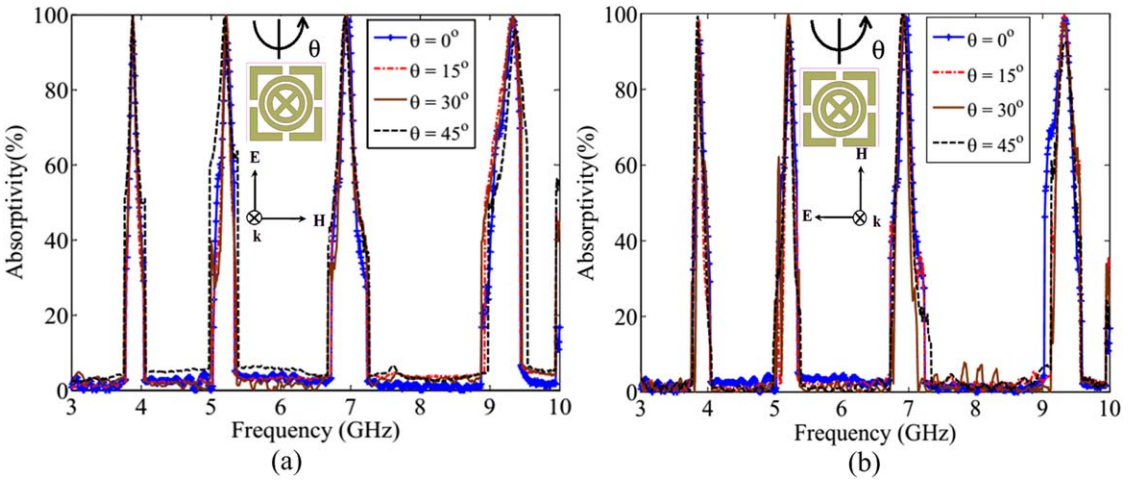

Figure 9 Measured absorptivity under oblique incidence condition for (a) TE and (b) TM polarizations. [Color figure can be viewed in the online issue, which is available at wileyonlinelibrary.com]

3. EXPERIMENTAL RESULTS

The proposed structure has been fabricated on a 230 × 230 mm^2 planar sheet of 1 mm thick FR-4 substrate using standard printed circuit board technology as shown in Figure 7(a). The reflection from the fabricated structure is measured inside anechoic chamber using two standard horn antennas LB-10180-SF (1–18 GHz) connected to an Agilent vector network analyzer N5230A which give rise to absorptivity. The experimental setup for measurement is shown in Figure 7(b).

Initially, an identical copper sheet has been placed in anechoic chamber and the reflection coefficient from the surface has been measured and used as a reference level. Next, the reflectance of the fabricated structure is measured and the difference between the measured responses provides the actual reflection from the structure. The measured result shows four distinct absorption peaks at 3.90, 5.20, 6.95, and 9.30 GHz with peak absorptivities of 94, 93.5, 98.8, and 98.6%, respectively, as shown in Figure 8(a). The slight deviation in absorption frequency could be due to fabrication imperfections.

To verify the polarization insensitivity of the fabricated structure, the sample has been rotated around its axis from 0° to 45° keeping the antennas fixed. The measured results, as shown in Figure 8(b), exhibit four distinct absorption peaks which match well with the simulated responses (shown in Fig. 3), thus verifying the polarization independence of the proposed structure.

Figure 9 shows the measured absorptivities for TE and TM polarizations with oblique incident angle ranging from 0° to 45°. In TE wave, the structure is kept fixed and the antennas have been rotated in such a way that the electric field direction is always kept constant and the magnetic field and wave vector directions have been changed by angle θ. Similarly, in case of TM wave, the magnetic field is maintained constant, whereas the other two vector directions have been rotated. In both the cases, the measured results are in good agreement with the simulated responses [shown in Figs. 4(a) and 4(b)] with a slight variation in absorption frequencies as shown in Figures 9(a) and 9(b).

4. CONCLUSION

An ultrathin quad-band MTM absorber structure with polarization insensitive as well as wide-angle absorption characteristics has been presented. Physical dimension of the proposed absorber is much smaller and compact compared to its counterparts due to the use of concentric square and circular rings. The outer square ring with four splits and two inner circular rings are designed in such a way which provides quad-band absorber application. The extra cross in the inner circular ring provides an alternative path for surface current flow, which makes the inner ring tunable for realizing the absorption frequency. The four splits in the outer square ring provide two discrete absorption frequencies, which can be explained from the surface current distributions in the metallic patches. The proposed structure shows nearly unity absorption for three different microwave bands (S, C, and X-band) aimed for radar applications. Moreover, the proposed structure is four-fold symmetric and shows polarization-insensitive behavior under normal incidence. The structure also shows high absorption (above 90%) under wide incident angles (0° to 45°) for both TE and TM polarizations. The absorber has been fabricated on a low cost commercially available FR-4 dielectric substrate and measured in anechoic chamber, therefore validating the quad-band performance. The dimensions of the proposed absorber structure can be easily tuned to other frequency spectrums covering various potential applications such as THz imaging, IR camouflage, and wireless communication.

ACKNOWLEDGMENTS

The authors want to acknowledge all the members of Microwave Metamaterial Laboratories and PCB fabrication laboratories for their continuous support. This work is partially supported by DRDO, India, under Project No. DLJ/TC/1025/I/30.

REFERENCES

1. D.R. Smith, W.J. Padilla, D.C. Vier, S.C. Nemat-Nasser, and S. Schultz, Composite medium with simultaneously negative permeability and permittivity, Phys Rev Lett 84 (2000), 4184.
2. N. Fang, H. Lee, C. Sun, and X. Zhang, Sub-diffraction-limited optical imaging with a silver superlens, Science 308 (2005), 534–537.
3. D. Schurig, J.J. Mock, B.J. Justice, S.A. Cummer, J.B. Pendry, A.F. Starr, and D.R. Smith, Metamaterial electromagnetic cloak at microwave frequencies, Science 314 (2006), 977–980.
4. S. Enoch, G. Tayeb, and P. Vincent, A metamaterial for directive emission, Phys Rev Lett 89 (2002), 3901–3904.
5. N.I. Landy, S. Sajuyigbe, J.J. Mock, D.R. Smith, and W.J. Padilla, Perfect metamaterial absorber, Phys Rev Lett 100 (2008), 207402.
6. S. Bhattacharyya and K.V. Srivastava, Ultra-thin metamaterial absorber using electric driven LC (ELC) resonator structure, In: Proceedings of Progress in Electromagnetics Research Symposium (PIERS), Kuala Lumpur, Malaysia, 2012, pp. 314–317.
7. S. Bhattacharyya, H. Baradiya, and K.V. Srivastava, An ultra-thin metamaterial absorber using electric driven LC resonator with

meander lines, In: IEEE International Symposium on Antennas and Propagation and USNC/URSI National Radio Science Meeting, Chicago, 2012, pp. 1–2.
8. S. Ghosh and K.V. Srivastava, Polarization insensitive tetra arrow metamaterial absorber, In: Proceedings of IEEE International Symposium on Antennas and Propagation and USNC-URSI National Radio Science Meeting in Orlando, Florida, 2013, pp. 1454–1455.
9. H. Tao, C.M. Bingham, D. Pilon, K.B. Fan, A.C. Strikwerda, D. shrekenhamer, W.J. Padilla, X. Zhang, and R.D. Averitt, A dual band terahertz metamaterial absorber, J Phys D 43 (2010), 225102.
10. S. Bhattacharyya and K.V. Srivastava, An ultra thin electric driven LC resonator structure as metamaterial absorber for dual band application, In: Proceeding of the International Synopsis of Electromagnetic Theory, Hiroshima, Japan, 2013, pp. 722–725.
11. S. Bhattacharyya, S. Ghosh, and K.V. Srivastava, Triple band polarization-independent metamaterial absorber with bandwidth enhancement at X-band, J Appl Phys 114 (2013), 094514.
12. S. Bhattacharyya and K.V. Srivastava, Triple band polarization-independent ultra-thin metamaterial absorber using ELC resonator, J Appl Phys 115 (2014), 064508.
13. S. Bhattacharyya, S. Ghosh, and K.V. Srivastava, Bandwidth enhanced metamaterial absorber using electric field driven LC resonator for airborne radar applications, Microwave Opt Technol Lett 55 (2013), 2131–2137.
14. S. Ghosh, S. Bhattacharyya, and K.V. Srivastava, Bandwidth-enhancement of an ultra-thin polarization insensitive metamaterial absorber, Microwave Opt Technol Lett 56 (2014), 350–355.
15. S. Ghosh, S. Bhattacharyya, and K.V. Srivastava, Bandwidth-enhanced polarization-insensitive microwave metamaterial absorber and its equivalent circuit model, J Appl Phys 115 (2014), 104503.
16. J. Sun, L. Liu, G. Dong, and J. Zhou, An extremely broad band metamaterial absorber based on destructive interference, Opt Express 19 (2011), 21155–21162.
17. Y.Z. Cheng, Y. Wang, Y. Nie, R.Z. Gong, X. Xiong, and X. Wang, Design, fabrication and measurement of a broadband polarization-insensitive metamaterial absorber based on lumped elements, J Appl Phys 111 (2012), 044902.
18. X.-J. He, Y. Wang, J.-M. Wang, and T.-L. Gui, Dual-band terahertz metamaterial absorber with polarization insensitivity and wide incident angle, Prog Electromagn Res 115 (2011), 381–397.
19. J.F. Federici, B. Schulkin, F. Huang, D. Gary, R. Barat, F. Oliveira, D. Zimdars, THz imaging and sensing for security applications-explosives, weapons and drugs, Semicond Sci Technol 20 (2005), S266–S280.
20. D. Zheng, Y. Cheng, D. Cheng, Y. Nie, and R. Gong, Four-band polarization-insensitive metamaterial absorber based on flower-shaped structures, Prog Electromagn Res 142 (2013), 221–229.
21. D.R. Smith, D.C. Vier, T. Koschny, and C.M. Soukoulis, Electromagnetic parameter retrieval from inhomogeneous metamaterials, Phys Rev E 71 (2005), 03661.
22. X. Shen, Y. Yang, Y. Zang, J. Gu, J. Han, W. Zhang, and T.J. Cui, Triple-band terahertz metamaterial absorber: Design, experiment and physical interpretation, Appl Phys Lett 101 (2012), 154102.

DESIGN OF A BROADBAND CIRCULARLY POLARIZED RECTENNA FOR MICROWAVE POWER TRANSMISSION

Chien-Hsing Lee and Yu-Han Chang
Department of Systems and Naval Mechatronic Engineering, National Cheng Kung University, Tainan 701, Taiwan, Republic of China; Corresponding author: chienlee@mail.ncku.edu.tw

Received 28 July 2014

ABSTRACT: *This article presents a broadband circularly polarized (CP) rectifying antenna (rectenna) for microwave power transmission at 4.2–7.6 GHz, comprising a broadband CP antenna, and a rectifier circuit. The antenna consists of a standard Schiffman phase shifter and a pair of orthogonally positioned linearly polarized slot antennas with equal radiation strength. The rectifier circuit is composed of a microwave Si Schottky detector diode (HSMS-2862), a low-pass filter, a load resistor, and a ripple capacitor. Output dc voltage of 1.98 V over a 680 Ω load resistance and the maximum microwave-to-dc conversion efficiency of 81.6 % were measured when 34 dBm microwave power was transmitted at 5.6 GHz over a distance of 50 cm.* © 2015 Wiley Periodicals, Inc. Microwave Opt Technol Lett 57:702–706, 2015; View this article online at wileyonlinelibrary.com. DOI 10.1002/mop.28931

Key words: *broadband circularly polarized antenna; phase shifter; rectenna*

1. INTRODUCTION

The development of modern technology for transmitting electrical power over free space was started in 1950's [1]. Since then, there have been a number of configurations proposed for the receiving device called rectenna (rectifying antenna) which is one of the most important components in the wireless power transmission. Although there are many well-known and well-established design methods and results of rectennas for wireless energy transfer [2–8], very few broadband rectennas [9–11] have been developed. A broadband rectenna is usually accomplished using a circularly polarized (CP) antenna array to receive energy from a system operating at different frequencies. However, its development and fabrication process are somewhat more difficult. This article proposes to use a broadband CP antenna for application involving microwave power transmission at 4.2–7.6 GHz based on the same structure and mechanism of the reported antenna [12]. The benefits for the use of this antenna are that it has good CP radiation patterns, steady radiation efficiency, good peak gain, and wider operating bandwidth. In addition, it has stable return loss since the rectifier circuit does not affect the impedance matching of the antenna.

To accomplish a broadband CP antenna, this study uses one Schiffman phase shifter (SPS) and a pair of orthogonally positioned linearly polarized (LP) slot antennas [12]. Since the implementation of a microstrip phase shifting circuit is difficult, a method that no additional conductor is required for the microstrip structure and is easy to fabricate without damaging the structure to fabricate a microstrip SPS has been proposed [13]. The overall size of the designed rectenna taken the feeding line into account as shown in Figure 1 is 125 × 70 mm^2, and it is printed on an FR4 substrate of thickness 1.6 mm with dielectric constant 4.4. As seen from Figure 1, a 50 mm long transmission line between the diode and the ripple capacitor is designed to prevent unnecessary current distribution from the radiation of horn antenna. The maximum path length of 50 mm that does not affect the measurement results is determined through trial and error.

2. DESIGN OF THE BROADBAND CP ANTENNA

2.1. Structure of the CP Antenna

The proposed CP antenna has a fed resistance to be 50 Ω by a microstrip line as shown in Figure 2. A pair of orthogonally positioned LP slot antenna is responsible for the horizontal and vertical radiations [14]. The low-frequency (i.e., 4.2 GHz) resonance path is at the outer end of the antenna portion and this low-frequency resonance point may be changed by varying the length of the sleeve as depicted in Figure 2. The U-shaped slot provides a path for the middle-and high-frequency (i.e., 5.6 and 7.4 GHz) resonances. The operating frequency range is